Hyper-Raman scattering from the incipient ferroelectric $KTaO_3$

Hans Vogt and Hiromoto Uwe*
Max-Planck-Institut für Festkörperforschung, Heisenbergstrasse 1, D-7000 Stuttgart 80, Federal Republic of Germany
(Received 23 September 1983)

Hyper-Raman scattering from $KTaO_3$ is studied to obtain the frequencies and linewidths of the seven optical Γ phonons with a high degree of accuracy. Particular attention is paid to the soft-mode region below 150 cm^{-1}. We confirm and extend the data found by electric-field-induced Raman spectroscopy. On the other hand, considerable discrepancies exist between hyper-Raman and infrared results. We also discuss the origin and temperature dependence of the hyper-Rayleigh line.

I. INTRODUCTION

Hyper-Raman (HR) spectroscopy[1] can be considered as a modulation technique which uses the electric field of a laser not only to excite the Raman process, but also to modulate the system under study. In this regard, it is quite similar to the electric-field-induced Raman effect[2] in which Raman-forbidden modes are made Raman-active by application of a static or low-frequency electric field. In comparing both methods, however, we notice two advantages of HR scattering:

(a) The elementary excitations to be observed are no longer influenced by the modulating electric field because they cannot follow the optical frequency.

(b) Electrodes and hence surface-layer problems are avoided.

On the other hand, both methods are limited by the threshold of dielectric breakdown, which often has the same order of magnitude and follows similar trends for laser radiation and low-frequency electric fields.[3] Thus materials suited for field-induced Raman spectroscopy are always good candidates for HR scattering and vice versa.

In the quantum picture, the HR effect is described as a three-photon process by which two incident photons are annihilated simultaneously to give rise to one scattered photon in the spectral region around the second harmonic of the exciting light. As an odd number of photons is involved, the parity-selection rule is the same as for infrared absorption. All infrared-active modes are also HR active. However, HR spectroscopy covers a broader range of symmetry types than any infrared method.[1,4]

Recently, the technique of HR scattering has been applied successfully to study the optical phonons in cubic $SrTiO_3$ (Refs. 5 and 6) and $BaTiO_3$.[7,8] Apart from structures which may result from perturbations of the O_h symmetry, these crystals do not show any first-order Raman spectrum. On the other hand, their first-order HR spectrum is comparatively intense and displays all the seven phonons at the Γ point of the Brillouin zone including the TO-LO splittings and the "silent" F_{2u} mode.

In the present paper we continue our study of perovskites and report on HR scattering from $KTaO_3$. As with $SrTiO_3$, this material is an incipient ferroelectric. Any ferroelectric long-range order is suppressed by dipolar fluctuations even at temperatures as low as 1.6 K.[9] In contrast to $SrTiO_3$, however, $KTaO_3$ preserves the cubic space-group symmetry O_h^1 ($Pm3m$) and does not undergo an antiferrodistortive phase transition. Owing to the unusually large polarizability, a static electric field of moderate strength can induce a variety of phenomena indicating the removal of inversion symmetry. Thus electric-field-induced piezoelectricity,[10,11] optical second-harmonic generation,[12] and first-order Raman scattering[2] have been observed. Moreover, ferroelectricity can be induced either by uniaxial stress[13] or by impurities replacing Ta or K ions.[14,15] Much interest has been attracted by the mixed-crystal series $KTa_{1-x}Nb_xO_3$ (KTN). Here, a transition to a low-temperature ferroelectric phase appears if the Nb concentration x exceeds the critical value of 0.08.[10] A comprehensive survey of works on $KTaO_3$ and KTN can be found in the introduction of Ref. 15.

The results of this paper are divided into three parts. First, we present room-temperature data from which we obtain accurate values of mode frequencies and damping constants. Applying the fluctuation-dissipation theorem, we derive the imaginary part of the dielectric function in the soft-mode region below 150 cm^{-1} and compare it with available infrared results. Then, attention is paid to the temperature dependence of the soft-mode parameters. We confirm and extend the data obtained by electric-field-induced Raman spectroscopy.[2] Comparing our values of the damping constant at low temperatures to those calculated from the far-infrared reflectivity, we find a discrepancy of an order of magnitude. Finally, we discuss the origin of the hyper-Rayleigh line and try to explain why its intensity increases with decreasing temperature.

II. EXPERIMENTAL DETAILS

HR scattering was excited by an acousto-optically Q-switched Nd-YAG laser ($\lambda_L = 1.06$ μm). At a repetition rate of 10 kHz, the laser pulses had a width of about 150 ns. A lens of $f = 6$ cm focused the laser beam into the sample. Without any crystal damage, the average power could be increased up to 3 W. We estimated the intensity at the focus to be several MW cm^{-2}. Details of our HR spectrometer have been described elsewhere.[16]

Measurements were performed on two single crystals of $KTaO_3$. They were grown from the melt by a top-seeded

TABLE I. Dispersion parameters of $KTaO_3$ at room temperature deduced from the hyper-Raman (HR, this work), the far-infrared reflectivity (IR, Refs. 18 and 19), and the electric-field-induced Raman spectrum (R, Ref. 2).

		Frequency (cm^{-1})			Linewidth, FWHM (cm^{-1})			Oscillator strength [contribution to $\epsilon(0)$]	
Mode	Symmetry	HR	IR[a]	R	HR	IR[b]	R	HR	IR[b]
TO1	F_{1u}	81	88	85	20	51;47	20	233	209.4;163
LO1		185	184		<6				
TO2	F_{1u}	199	199	198 (10 K)	<6	2.4;11		6.5	5.0;7.6
LO2	F_{2u}	279							
TO3	F_{2u} (silent)	279							
LO3		422	421		7				
TO4	F_{1u}	546	547	556 (10 K)	15	24		2.5	2.4
LO4		826	838		20				

[a]Reference 18.
[b]Reference 19.

solution method.[13] After being sawed and ground to cubic samples with (100) surfaces they were mounted in a continuous-flow cryostat and cooled by helium exchange gas. The temperature was kept constant within ± 0.5 K and could be varied between 15 and 295 K. The lower limit was set by the absorption of laser stray light within the cryostat. A Chromel-Au(Fe) thermocouple directly contacting the sample measured the temperature. Below 100 K, however, we could also calculate the temperature from the anti-Stokes- to Stokes-intensity ratio of the soft mode with sufficient accuracy. The HR and thermocouple values differed by less than 1 K, except for the two lowest temperatures where the difference reached 3 K. We concluded that the samples were almost free of temperature gradients and did not absorb an appreciable amount of laser light.

The spectral slit width was adjusted to the intensity of the HR lines under study and varied between 1 and 6 cm^{-1}. The photon counting time per spectral element was usually 100, but sometimes 500 s.

III. HYPER-RAMAN SPECTRA AT ROOM TEMPERATURE

Figure 1 shows a complete first-order HR spectrum of $KTaO_3$ at room temperature. We have chosen the scattering configuration $y(xy)x$, where y and x stand for cubic axes. It is the simplest geometry that permits the observation of all the seven optical Γ phonons. As shown by the inset, the spectrum between 150 and 300 cm^{-1} has been repeated with a higher spectral resolution and clearly reveals three HR lines. Following the notation of Cowley,[17] we have numbered the phonons in order of increasing frequencies. LO and TO modes have been distinguished by comparing Fig. 1 with the spectrum obtained in the backscattering configuration $x(yy)\bar{x}$. As predicted by the form of the HR tensors,[5] only the lines of the three phonons TO1, TO2, and TO4 are left in this geometry.

Frequencies and linewidths have been listed in Table I, together with infrared[18,19] and Raman[2] data. Our value of the silent-mode frequency is quite close to the value of 274 cm^{-1} found by Raman spectroscopy in the stress-induced ferroelectric phase at 2 K.[13] Using the Lyddane-Sachs-Teller (LST) relation, we can calculate the static dielectric constant $\epsilon(0)$. With $\epsilon(\infty)=4.592$,[20] we obtain $\epsilon(0)=247$, whereas capacitance measurements yield values between 239 and 243.[21–23] From the TO-LO splittings we can estimate the oscillator strengths of the three infrared-active modes.[5,24] These values are also quoted in Table I.

We have concentrated on the low-frequency part of the HR-spectrum with particular accuracy. Figure 2 shows the Stokes and anti-Stokes line of the soft TO1 mode at room temperature measured in the backscattering configuration $x(yy)\bar{x}$. The shape of the weaker hyper-Rayleigh line coincides with the instrumental function of the double monochromator. As in the case of $SrTiO_3$,[5] the fluctuation-dissipation theorem can be used to relate the HR spectrum to the imaginary part $\epsilon''(\Omega)$ of the dielectric function. On the Stokes side the HR efficiency S is given by

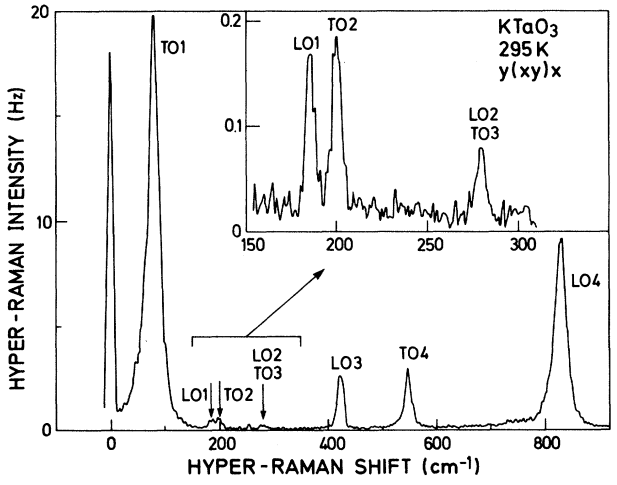

FIG. 1. Hyper-Raman spectrum of $KTaO_3$ at room temperature displaying the seven optical Γ phonons.

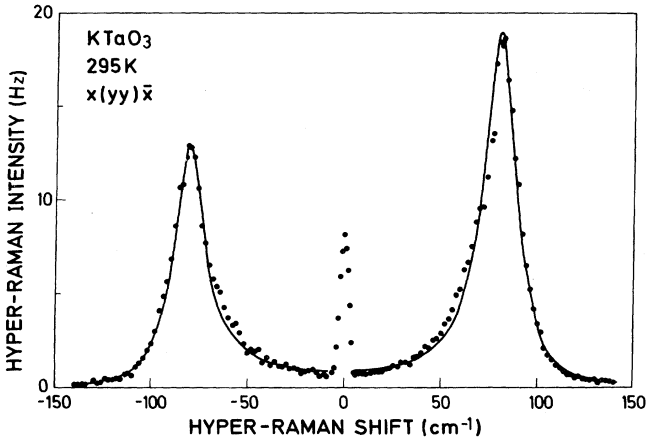

FIG. 2. Stokes and anti-Stokes line of the soft mode at room temperature. (Closed circles, experiment; solid line, classical dispersion formula.)

$$S(2\omega_L-\Omega)=A_{yy}[n(\Omega)+1]\epsilon''(\Omega)\,, \tag{1}$$

where ω_L is the laser frequency, Ω the HR shift, $n(\Omega)$ the Bose-Einstein population factor, and A_{yy} a coefficient independent of Ω. Replacing $[n(\Omega)+1]$ by $n(\Omega)$, we obtain the HR efficiency $S(2\omega_L+\Omega)$ on the anti-Stokes side. In Fig. 3 we have plotted $\epsilon''(\Omega)$ as derived from the experimental points of Fig. 2. In order to calibrate $\epsilon''(\Omega)$, use has been made of the Kramers-Kronig relation and the oscillator strength of the TO1 mode quoted in Table I [see Eq. (11) in Ref. 5]. For comparison, Fig. 3 also shows the results of three infrared reflectivity studies.[19,25,26] We find a similar discrepancy as in $SrTiO_3$ (Ref. 5). HR scattering reveals a much sharper resonance than infrared spectroscopy.

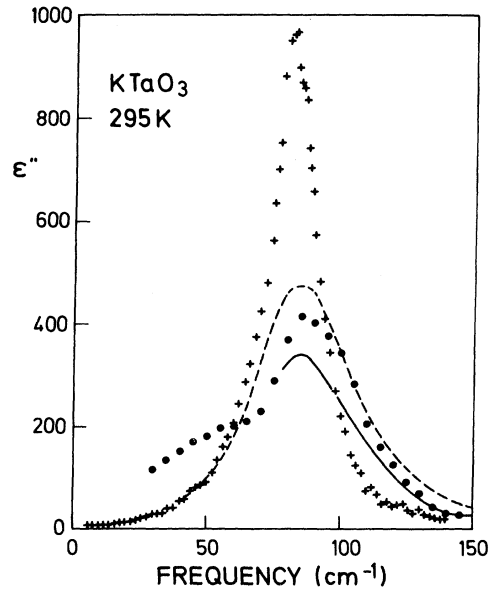

FIG. 3. Imaginary part of the far-infrared dielectric function. (Crosses, this work; solid line, Ref. 19; dashed line, Ref. 25; closed circles, Ref. 26.)

The profile of the TO1 line closely follows a classical dispersion formula, i.e.,

$$\epsilon''(\Omega)=\frac{4\pi\rho\Omega_0^2\gamma\Omega}{(\Omega_0^2-\Omega^2)+\gamma^2\Omega^2}\,, \tag{2}$$

where $4\pi\rho$ is the oscillator strength, Ω_0 the mode frequency, and γ the damping constant. The adequacy of Eq. (2) is demonstrated by the solid line in Fig. 2. Here, we have avoided a least-squares fit, but have just used the position of the maximum as Ω_0 and the linewidth as γ.

IV. SOFT-MODE SPECTROSCOPY

Figure 4 shows the frequency Ω_0 and the damping constant γ of the soft phonon as functions of temperature. Our values (closed circles) are compared with the results of electric-field-induced Raman spectroscopy (crosses).[2]

At low temperatures γ becomes so small that the "true" line shape must be deconvoluted from the measured one. An example is given in Fig. 5. We have assumed a convolution of the HR efficiency as described by Eqs. (1) and (2) with a triangular instrumental profile the width of which can be taken from the hyper-Rayleigh line. Besides the three soft-mode parameters $4\pi\rho A_{yy}$, Ω_0, and γ we have adjusted the temperature T in the Bose-Einstein popula-

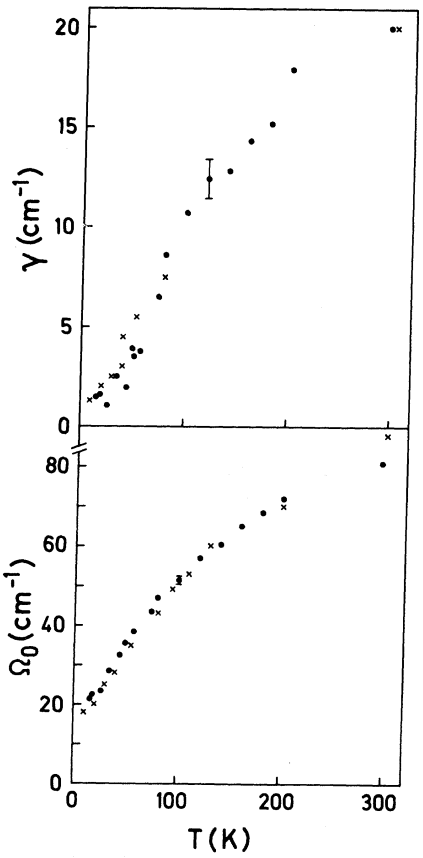

FIG. 4. Frequency Ω_0 and damping constant γ of the soft mode as a function of temperature. (Closed circles, this work; crosses, Ref. 2.)

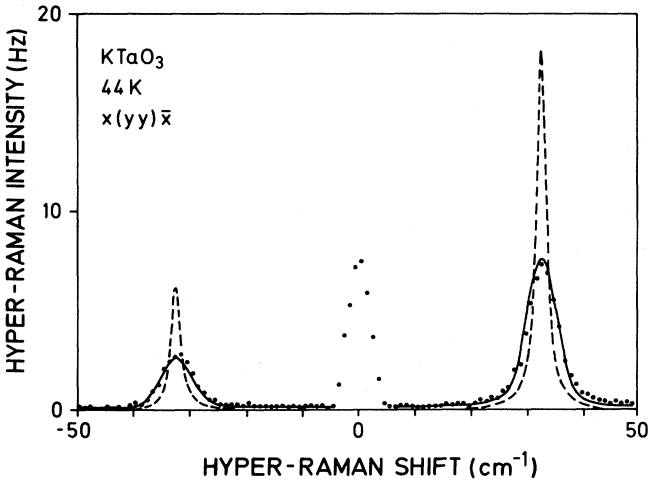

FIG. 5. Deconvolution of the true soft-mode line shape from the measured one. (Dots, experimental values; solid line, least-squares fit; dashed line, deconvoluted line.)

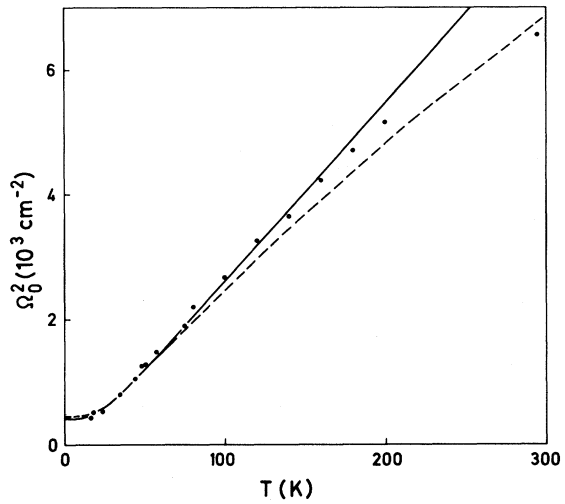

FIG. 6. Square of the soft-mode frequency as a function of temperature. [Dots, hyper-Raman values; dashed line, calculated from the dielectric data of Ref. 23 with the use of the Lyddane-Sachs-Teller relation; solid line, least-squares fit of Barrett's formula for $\epsilon(0)$ to the hyper-Raman values of Ω_0^2.]

tion factor. The solid curve in Fig. 5 represents a least-squares fit to the experimental points, while the dashed curve describes the deconvoluted or true line shape. In calculating the quantity to be minimized by the fitting procedure, we have weighted the squares of the deviations by the squares of the experimental values. Thus we have given preference to the maximum, rather than to the wings, of the soft-mode line.

According to Fig. 4, HR and electric-field-induced Raman spectroscopy lead to almost the same results. In particular, we confirm that light scattering yields a much smaller damping constant than far-infrared reflectivity.[25] The reason for this discrepancy may be found either in the inaccuracy of infrared measurements at very low wave numbers or in the influence of surface conditions, especially surface layers.[20,27] The second possibility must be taken into account because the penetration depth of far-infrared radiation in perovskites is extremely small. On the other hand, light scattering techniques certainly reveal bulk properties.

In Fig. 6 we have plotted the square of the soft-mode frequency as a function of temperature. The dashed and solid curves have been obtained by combining the LST relation and the temperature dependence of the static dielectric constant $\epsilon(0)$. We have written

$$\Omega_0^2=\epsilon(\infty)\frac{\Omega_{\mathrm{LO1}}^2\Omega_{\mathrm{LO3}}^2\Omega_{\mathrm{LO4}}^2}{\Omega_{\mathrm{TO2}}^2\Omega_{\mathrm{TO4}}^2}\left[\frac{1}{\epsilon(0)}\right], \tag{3}$$

assuming all factors in front of $1/\epsilon(0)$ as independent of temperature. At low temperatures $\epsilon(0)$ does not follow a Curie-Weiss law, but can be fairly well described by Barrett's formula,[28] i.e.,

$$\epsilon(0)=A+B\left[\tfrac{1}{2}T_1\coth\left[\frac{T_1}{2T}\right]-T_0\right]^{-1}. \tag{4}$$

Although the physical significance of this expression is questionable,[14] several authors have fitted successfully the four parameters A, B, T_1, and T_0 to their dielectric susceptibility data.[23,29–31] The dashed curve in Fig. 6 refers to the set of parameters found by Samara and Morosin,[23] while the solid curve is a least-squares fit to our data. Of course, the temperature range above 200 K is not weighted properly by our fitting procedure because there is only one experimental point. Values of the four parameters are listed in Table II.

V. NOTE ON HYPER-RAYLEIGH SCATTERING

Figure 7 presents the integrated hyper-Rayleigh intensity as a function of temperature. The curve refers to the scattering configuration $x(yy)\bar{x}$ and was obtained in a run separate from the HR measurements. The increase below 100 K can be approximately described by an exponential law of the form $T^{-2.5}$. The hyper-Rayleigh line shape always coincides with the instrumental profile. As symmetry forbids any coupling between the hyperpolarizability and acoustic phonons or entropy fluctuations,[16] it is most probable that the observed hyper-Rayleigh scattering does not represent a central peak of dynamical origin, but arises from coherent optical second-harmonic generation (SHG). Although $KTaO_3$ is a centrosymmetric crystal, there are several sources of SHG. At this stage, however, we are not able to discriminate between them. Therefore we just quote three different mechanisms and suggest further experiments:

TABLE II. Parameters of Barrett's formula for the static dielectric constant $\epsilon(0)$.

	A	B (K)	T_1 (K)	T_0 (K)
Reference 23	47.5	5.45×10^4	56.9	13.1
This work	0	5.58×10^4	54.2	12.9

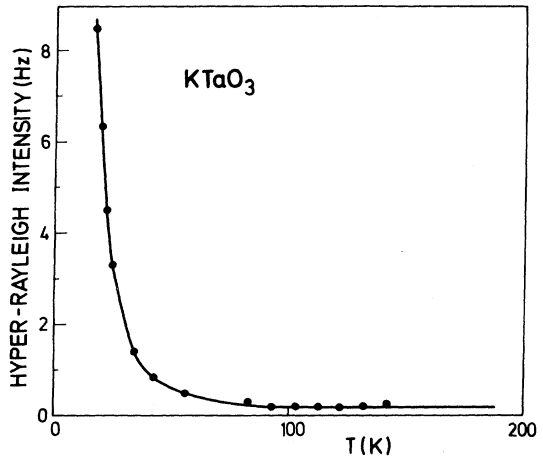

FIG. 7. Hyper-Rayleigh intensity as a function of temperature. The scattering geometry is $x(yy)\bar{x}$.

(i) In centrosymmetric crystals, SHG can arise from a nonlinear polarization being proportional to the product of the electric field and its spatial gradient. The nonlinear susceptibility involved is a tensor of fourth rank and thus exists in the presence of inversion symmetry.[32] In their study of the electric-field-induced SHG in $KTaO_3$, Fujii and Sakudo[12] referred to this spatial dispersion phenomenon in order to explain the small SHG intensity at zero-applied field. Detailed measurements of Maker fringes are needed to ascertain this point of view. However, it will be difficult to explain the temperature dependence shown in Fig. 7.

(ii) Our samples are not free of internal uniaxial stresses. Locally, these may exceed the critical value σ_c above which $KTaO_3$ becomes ferroelectric.[13] Thus, polarized regions are formed. Their number and dimension increase with decreasing temperature because σ_c decreases in approaching the virtual phase transition. If the observed SHG results from stress-induced ferroelectricity, we expect a temperature dependence as shown in Fig. 7. Lengthy and repeated annealing of the samples will indicate the influence of internal stresses on SHG.

(iii) From their thermal conductivity measurements Salce *et al.*[33] concluded that residual and unavoidable amounts of Nb and Na induce extended dipolar defects. These may also be regarded as sources of SHG. As they expand with decreasing temperature, we expect a corresponding increase in SHG intensity in agreement with Fig. 7. Measurements on doped samples with well-defined low concentrations of Nb and Na will show the influence of impurities on SHG.

ACKNOWLEDGMENTS

The authors wish to thank W. Kress and G. Kugel for stimulating discussions and M. Cardona for a critical reading of the manuscript. The technical assistance of H. Hirt and P. Wurster is gratefully acknowledged.

*On leave from the Institute of Applied Physics, University of Tsukuba, Sakura, Ibaraki 305, Japan.

[1]H. Vogt, in *Light Scattering in Solids II*, Vol. 50 of *Topics in Applied Physics*, edited by M. Cardona and G. Güntherodt (Springer, Berlin, 1982), p. 207.
[2]P. A. Fleury and J. M. Worlock, Phys. Rev. 174, 613 (1968).
[3]N. Bloembergen, IEEE J. Quantum Electron. QE-10, 375 (1974).
[4]S. J. Cyvin, J. E. Rauch, and J. C. Decius, J. Chem. Phys. 43, 4083 (1965).
[5]H. Vogt and G. Rossbroich, Phys. Rev. B 24, 3086 (1981).
[6]K. Inoue, N. Asai, and T. Sameshima, J. Phys. Soc. Jpn. 50, 1291 (1981).
[7]H. Vogt, J. A. Sanjurjo, and G. Rossbroich, Phys. Rev. B 26, 5904 (1982).
[8]K. Inoue and S. Akimoto, Solid State Commun. 46, 441 (1983).
[9]S. H. Wemple, Phys. Rev. 137, A1575 (1965).
[10]D. Rytz, A. Châtelain, and U. T. Höchli, Phys. Rev. B 27, 6830 (1983).
[11]A. M. Raaen and K. Fossheim, J. Phys. C 13, 283 (1980).
[12]Y. Fujii and T. Sakudo, Phys. Rev. B 13, 1161 (1976).
[13]H. Uwe and T. Sakudo, J. Phys. Soc. Jpn. 38, 183 (1975); Phys. Rev. B 15, 337 (1977).
[14]U. T. Höchli and L. A. Boatner, Phys. Rev. B 20, 266 (1979).
[15]R. L. Prater, L. L. Chase, and L. A. Boatner, Phys. Rev. B 23, 221 (1981).
[16]H. Vogt and G. Neumann, Phys. Status Solidi B 92, 57 (1979).
[17]R. A. Cowley, Phys. Rev. 134, A981 (1964).
[18]C. H. Perry and N. E. Tornberg, Phys. Rev. 183, 595 (1969).
[19]R. C. Miller and W. G. Spitzer, Phys. Rev. 129, 94 (1963).
[20]Y. Fujii and T. Sakudo, J. Phys. Soc. Jpn. 41, 888 (1976).
[21]G. Rupprecht and R. O. Bell, Phys. Rev. 135, A748 (1964).
[22]S. H. Wemple, Phys. Rev. 137, A1575 (1965); S. H. Wemple, A. Jayaraman, and M. DiDomenico, Jr., Phys. Rev. Lett. 17, 142 (1966).
[23]G. A. Samara and B. Morosin, Phys. Rev. B 8, 1256 (1973).
[24]J. L. Servoin, Y. Luspin, and F. Gervais, Phys. Rev. B 22, 5501 (1980).
[25]C. H. Perry and T. F. McNelly, Phys. Rev. 154, 456 (1967).
[26]K. F. Pai, T. J. Parker, N. E. Tornberg, R. P. Lowndes, and W. G. Chambers, Infrared Phys. 18, 327 (1978).
[27]J. P. Ansermet, D. Rytz, A. Châtelain, U. T. Höchli, and H. E. Weibel, J. Phys. C 14, 4541 (1981).
[28]J. H. Barrett, Phys. Rev. 86, 118 (1952).
[29]W. R. Abel, Phys. Rev. B 4, 2696 (1971).
[30]R. P. Lowndes and A. Rastogi, J. Phys. C 6, 932 (1973).
[31]D. Rytz, U. T. Höchli, and H. Bilz, Phys. Rev. B 22, 359 (1980).
[32]L. Ortmann and H. Vogt, Opt. Commun. 16, 234 (1976).
[33]B. Salce, A. M. De Goer, and L. A. Boatner, J. Phys. (Paris) Colloq. 42, C6-430 (1981).